Nanobody®-based chromatin immunoprecipitation/ micro-array analysis for genome-wide identification of transcription factor DNA binding sites

Trong Nguyen-Duc[1,2], Eveline Peeters[3], Serge Muyldermans[1,2,*], Daniel Charlier[3] and Gholamreza Hassanzadeh-Ghassabeh[1,2]

[1]Research group of Cellular and Molecular Immunology, Vrije Universiteit Brussel, Pleinlaan 2, B-1050 Brussel, Belgium, [2]Department of Structural Biology, VIB, B-1050 Brussels, Belgium and [3]Research group of Microbiology, Vrije Universiteit Brussel, Pleinlaan 2, B-1050 Brussel, Belgium

ABSTRACT

Nanobodies® are single-domain antibody fragments derived from camelid heavy-chain antibodies. Because of their small size, straightforward production in *Escherichia coli*, easy tailoring, high affinity, specificity, stability and solubility, nanobodies® have been exploited in various biotechnological applications. A major challenge in the post-genomics and post-proteomics era is the identification of regulatory networks involving nucleic acid–protein and protein–protein interactions. Here, we apply a nanobody® in chromatin immunoprecipitation followed by DNA microarray hybridization (ChIP-chip) for genome-wide identification of DNA–protein interactions. The Lrp-like regulator Ss-LrpB, arguably one of the best-studied specific transcription factors of the hyperthermophilic archaeon *Sulfolobus solfataricus*, was chosen for this proof-of-principle nanobody®-assisted ChIP. Three distinct Ss-LrpB-specific nanobodies®, each interacting with a different epitope, were generated for ChIP. Genome-wide ChIP-chip with one of these nanobodies® identified the well-established Ss-LrpB binding sites and revealed several unknown target sequences. Furthermore, these ChIP-chip profiles revealed auxiliary operator sites in the open reading frame of *Ss-lrpB*. Our work introduces nanobodies® as a novel class of affinity reagents for ChIP. Taking into account the unique characteristics of nanobodies®, in particular, their short generation time, nanobody®-based ChIP is expected to further streamline ChIP-chip and ChIP-Seq experiments, especially in organisms with no (or limited) possibility of genetic manipulation.

INTRODUCTION

Chromatin immunoprecipitation (ChIP) is a widely used technique to measure DNA-binding events of transcription factors *in vivo*. ChIP, combined with DNA micro-array analysis (ChIP-chip) or high-throughput sequencing (ChIP-Seq), allows genome-wide mapping of all locations where a factor is associated, through protein–DNA or protein–protein interactions (1,2). In contrast to transcriptomics and proteomics that measure the consequences of the regulatory interactions (changes in RNA or protein levels), which may be because of either direct or indirect (cascade) effects, ChIP-chip and ChIP-Seq provide information on the regulatory interactions themselves and are, therefore, the most direct ways to define regulons. An additional advantage of ChIP-chip and ChIP-Seq is that the analysis can be performed in a wild-type strain; there is no need for a gene disruption mutant or a strain that overexpresses a tagged regulatory DNA-binding protein. The ChIP-chip procedures have been established for different organisms, ranging from prokaryotes and yeasts to higher eukaryotes, including mammals (3–9). In bacteria, ChIP-chip has been applied mainly to *Escherichia coli* (10,11). The use of ChIP in archaea has been lagging behind and, to our knowledge, has only been applied to *Halobacterium salinarum NRC-1* (12–14).

A ChIP-chip assay consists of multiple sequential experimental steps. Living cells are first treated with

formaldehyde, resulting in covalent cross-linking of DNA-associated proteins to DNA. Subsequently, nucleoprotein is extracted and sheared into shorter DNA fragments, usually by sonication. This preparation is then subjected to immunoprecipitation using an antibody specific for the protein of interest. After ChIP, the enriched nucleoprotein complexes are treated to hydrolyse the cross-linked complexes, and DNA is purified. Generally, the yield of ChIP DNA is too low and needs to be amplified before array hybridization. Given the large number of experimental parameters in a ChIP-chip experiment, it is not surprising that there is a wide variation in the design of different studies. One of the most critical determinants of a successful ChIP-based approach is the antibody (5,11,15,16). ChIP antibodies should be capable of capturing specifically one single protein of a vast pool of DNA-binding proteins. It should also be considered that DNA binding and DNA–protein cross-linking might provoke conformational changes in the nucleoprotein complexes that lead to epitope masking, causing false-negative outcomes, whereas cross-reactivity of the antibodies to non-cognate targets could generate false-positive outcomes. Effects of epitope masking can be minimized by using polyclonal antibodies (pAbs) (17). However, pAbs increase the frequency of false-positive outcomes, their production requires regular immunization and they exhibit batch to batch variability (18,19). In comparison with pAbs, monoclonal antibodies (mAbs) suffer less from the aforementioned problems. However, the availability of high-quality ChIP-grade mAbs is apparently limited (11,20). Epitope tagging, by homologous recombination-mediated knock-in of the tagged genes, could circumvent the lack of ChIP-grade mAbs. Although this technology is relatively straightforward for some well-established model organisms, such as *Saccharomyces cerevisiae* and *E. coli* (7,8,14,21–23), genetic tools to achieve this in many organisms such as *Sulfolobus*, one of the archaeal model organisms, are still limited (24,25). Moreover, it is not excluded that the characteristics (e.g. stability, folding efficiency, hydrophobicity) of a tagged protein may differ from those of the wild-type. Evidently, such potential differences can affect the outcome of the ChIP experiment.

Monospecific antigen-binding domains can also be produced by microorganisms at a fraction of the cost of mAbs, and they might constitute a novel and valuable resource of ChIP-grade antibodies. Especially the recombinant single-domain antigen-binding fragments, such as Nanobodies®, seem to be attractive for ChIP. Remarkably, the antibody repertoire of camelids contains, in addition to conventional antibodies, a novel class of antibodies comprising heavy chains only (26). These antibodies, referred to as heavy-chain antibodies, bind their cognate antigen by virtue of one single-variable domain, termed VHH or nanobody®. In contrast, the antigen binding by conventional antibodies relies on variable regions of both heavy and light chains (VH and VL, respectively). Therefore, construction of libraries of antigen-binding domains of conventional antibodies involves random association of VHs and VLs. Consequently, large libraries are required to restore all possible VH–VL combinations, of which some may represent the original VH–VL pairing as it was affinity matured *in vivo* during immunization with antigen. As camelid heavy-chain antibodies bind their target antigens by only one single domain, construction of large immune libraries to trap antigen-specific nanobodies® has proven unnecessary (27,28). Construction of libraries of antigen-binding repertoire of conventional antibodies is also complicated by the existence of multiple VH and VL gene families, whereas the vast majority of VHHs belong to one single sub-family (28). The aforementioned technological advantages of constructing 'immune' nanobody® libraries, together with small size, recognition of unique epitopes, high affinity, high solubility, high expression yield in heterologous expression systems and easy tailoring, make nanobodies® an interesting class of affinity reagents for various applications (27,29,30).

Here, we demonstrate the use of target-specific nanobodies® in ChIP experiments. As a model system, we chose the well-characterized transcription regulator Ss-LrpB from the hyperthermoacidophilic archaeon *Sulfolobus solfataricus* (31). Ss-LrpB belongs to the leucine-responsive regulatory protein (Lrp) family, a widespread and abundant family of regulators in prokaryotes, both bacteria and archaea (32,33). Several regulatory targets of Ss-LrpB have already been identified by *in vitro* binding experiments and by *in vivo* gene expression analysis (34). These targets include the regulator gene itself and a gene cluster juxtaposed to it, encoding a putative ferredoxin oxidoreductase and two permeases. In this work, different Ss-LrpB-specific nanobodies® were generated and assessed for their capacity to capture specifically the regulator, either free or bound to DNA. We then developed a nanobody®-based ChIP protocol for *S. solfataricus*. The genome-wide application of nanobody®-based ChIP for Ss-LrpB is demonstrated by implementation of the Roche NimbleGen™ microarray platform. The results presented here demonstrate the utility and specificity of nanobodies® as a novel class of affinity reagents for ChIP.

MATERIALS AND METHODS

Protein purifications

Full-length non-tagged Ss-LrpB protein was produced recombinantly in *E. coli* and was purified by heat treatment and ion exchange chromatography, as previously described (35). The His-tagged C-terminal domain of Ss-LrpB was purified by Ni^{2+} affinity chromatography (36). LysM and Ss-Lrp proteins were produced and purified by the same procedure as the Ss-LrpB purification. For LysM, *E. coli* BL21(DE3) was first transformed with construct pLUW632 (37). After purification, the Ss-LrpB and Ss-Lrp preparations were dialysed against 20 mM of Tris–HCl (pH 8.0), 50 mM of NaCl, 0.4 mM of ethylenediaminetetraacetic acid (EDTA), 0.1 mM of DTT, 12.5% of glycerol and the LysM preparation against 20 mM of Tris–HCl (pH 8.0) and 20% of glycerol.

After identification as described later in the text, the Ss-LrpB-specific VHH (nanobody®) genes were cloned into the pHEN6c vector, which allows expression of nanobodies® in fusion with His_6 tag (38). Expression and purification of nanobodies® were performed as previously described (39).

Protein concentrations in the case of Ss-LrpB expressed in monomeric units were determined by ultraviolet absorption at 280 nm and by densitometric analysis of Coomassie stained sodium dodecyl sulphate (SDS)–polyacrylamide gel (PAG).

Generation of Ss-LrpB-specific nanobodies®

Ss-LrpB-specific nanobodies® were generated by immunizing an alpaca (*Vicugna pacos*) with purified full-length Ss-LrpB. Using peripheral blood lymphocytes of the animal, a VHH library was constructed, and specific nanobodies® were selected according to published methods (38).

Surface plasmon resonance

Surface plasmon resonance (SPR) measurements of the interactions of Ss-LrpB-specific nanobodies® with their antigen were performed with a Biacore T200 instrument. All measurements were performed in phosphate-buffered saline (PBS) at 25°C. CM5 chips (GE Healthcare) were used to covalently couple Ss-LrpB via its primary amines of lysine residues. Ss-LrpB was immobilized onto the chip until the signal reached 500 resonance units (RUs). Measurements were performed by applying various concentrations of nanobodies® (between 3 and 500 nM) as analyte to the chip, at a flow rate of 30 μl/min. An association phase of 150 s was followed by a dissociation phase of 600 s. Regeneration was achieved by washing the chip with 10 mM of glycine hydrochloride (pH 2.0) for 20 s, at a flow rate of 60 μl/min. The association and dissociation curves of the sensorgrams were analysed with the Biacore Evaluation software, version 2.0, yielding kinetic and equilibrium binding constants. Epitope analysis was done with 250, 500 or 750 nM of each nanobody®, either alone or combined, also at a flow rate of 30 μl/min. Each association phase lasted 200 s.

Immunoprecipitation (pull-down) assays with crude cell extracts

Escherichia coli BL21(DE3) crude cell extracts containing one of the three Lrp-like transcription factors from *S. solfataricus* (Ss-LrpB, LysM or Ss-Lrp), expressed from recombinant pET24 vectors, were used for these experiments. Crude extracts from BL21(DE3) containing an empty pET24 vector served as negative control. Cell pellets from 20 ml cultures were resuspended in 1 ml of IP buffer [150 mM of NaCl, 50 mM of Tris–HCl (pH 8.0), 1% of Triton X-100, 0.5% of NP-40, 1% of deoxycholate], sonicated and centrifuged. Aliquots of 200 μl of the supernatants were incubated with different amounts of His-tagged nanobodies® for 20 min at room temperature. Subsequently, the pull-down was performed using Nickel-NTA magnetic particles (Bio-Nobile) following supplier's recommendations. The nanobody®–antigen complexes were eluted with 100 μl of PBS containing 250 mM of imidazole, and the eluted proteins were analysed using 12% of SDS–PAG electrophoresis (PAGE).

Native protein polyacrylamide gel electrophoresis

Native protein gel electrophoresis was performed with 10% of Tris–glycine gel (Invitrogen). Each reaction mixture, with a total volume of 20 μl, contained 20 μg of Nb9 and/or ~10 μg of the respective Lrp-like protein. Reaction mixtures were incubated for 30 min at room temperature before gel analysis. The electrophoresis was performed in Tris–glycine (pH 8.5) electrophoresis buffer at 125 V for 4–5 h. The gel was stained with Coomassie blue.

Electrophoretic mobility shift assays

Electrophoretic mobility shift assays (EMSAs) were performed with labelled DNA prepared by polymerase chain reaction (PCR). One of the two oligonucleotides was 5′-end labelled with ^{32}P using $[\gamma-^{32}P]$-adenosine triphosphate (Perkin Elmer) and T4 polynucleotide kinase (Fermentas). The PCR mixtures contained Taq DNA polymerase (Ready Mix, Sigma-Aldrich), the labelled primer, a second non-labelled primer and the recombinant vector pUC18^P/$_o$ *Ss-lrpB* or pBendBox1 as template (31). Primer sequences are given in Supplementary Table S1. Labelled DNA fragments were purified from PAG. EMSA experiments were performed as previously described (40). Binding reactions were allowed to equilibrate for 20 min at 37°C in Lrp-binding buffer [20 mM of Tris–HCl (pH 8.0), 1 mM of $MgCl_2$, 50 mM of NaCl, 0.4 mM of EDTA, 0.1 mM of DTT, 12.5% of glycerol]. For binding reactions in which Ss-LrpB and nanobodies® were combined, Ss-LrpB was pre-incubated with DNA for 20 min before addition of nanobody®.

Cell culture and formaldehyde cross-linking

Sulfolobus solfataricus P2 (DSMZ 1617) was cultured aerobically by shaking at 80°C in Brock medium (41) supplemented with 0.1% of tryptone as carbon and nitrogen source. Depending on the downstream application, 50 ml or 200 ml cultures were grown. When cells were in mid-exponential growth phase [at optical density $(OD)_{600 nm}$ of 0.5], the cultures were cooled to 37°C, and formaldehyde was added to a final concentration of 1%, while shaking for 5 min, unless otherwise noted. The cross-linking reaction was quenched by adding glycine to a final concentration of 125 mM, followed by an additional incubation of 5 min at 37°C.

To find the optimal cross-linking time, 50 ml cultures were formaldehyde-treated for different periods, centrifuged and sonicated for 5 min (see later in the text for sonication details). After this treatment, 200 μl aliquots were subjected to phenol extraction to separate protein-free from complexed DNA. This extraction was done by mixing with 2 volumes of phenol/chloroform/isoamyl alcohol (25:24:1) followed by 5 min of centrifugation at

20 817*g*. The protein-free DNA fractions were recovered from the upper aqueous phase by ethanol precipitation. Finally, the extracted DNA was treated with 16.5 ng RNase (Invitrogen) for 2 h at 37°C and column-purified. The degree of cross-linking was assessed by quantitative PCR (qPCR) analysis of the protein-free DNA samples relative to DNA from a non–cross-linked sample, which represented total DNA, and was prepared by extraction and purification as described for cross-linked samples.

Sonication

Cross-linked cells from either 50 ml or 200 ml cultures were centrifuged at 3220*g* for 10 min; cell pellets were washed twice with PBS and resuspended in 3 ml IP buffer. Sonication was performed with a Bioblock Scientific-Vibracell sonicator at 20% of the maximal amplitude, in a pulsed operating mode with 9 s rest in between each 3 s of operation. The total operating time was 9 min, unless otherwise stated. Cells were continuously cooled during sonication. After sonication, the samples were centrifuged at 21 000*g* for 15 min, and the supernatants were used for ChIP as described later in the text.

For small-scale sonication tests, samples from 50 ml cultures were cross-linked for 5 min and sonicated with total operation times between 3 and 30 min. For each sample, a 200 μl aliquot was purified by phenol extraction, and a 200 μl aliquot was de-cross-linked, as described later in the text. These two samples, corresponding to protein-free DNA and total genomic DNA, respectively, were analysed by qPCR to calculate the ratio of cross-linked protein–DNA complexes versus total DNA. The DNA size distribution was analysed by 1% agarose gel electrophoresis of de-cross-linked samples.

Chromatin immunoprecipitation

For each ChIP assay, 0.5 mg of purified nanobody® was added to 3 ml cross-linked sonicated sample obtained as previously described after centrifugation. The mixtures were incubated overnight at 4°C. In parallel, 1 ml of His-Select™ Nickel Affinity Gel suspension (Sigma-Aldrich) was blocked overnight at 4°C with IP buffer containing 0.5% of bovine serum albumin, and it was added the next day to the mixtures of the nanobody®–cross-linked/sonicated sample. After 2 h incubation at room temperature, the gel pellets were washed three times with 4 ml of IP buffer each. The ChIP-enriched fractions were then eluted from the gel pellet by the addition of 400 μl of elution buffer [50 mM of Tris–HCl (pH 8.0), 1% of Triton X-100, 0.5% of NP-40, 1% of deoxycholate, 1% of SDS, 300 mM of NaCl, 250 mM of imidazole] and a further incubation of the gel mixture at room temperature for 1 h. Subsequently, 400 μl samples were subjected to de-cross-linking by incubation at 55°C for 16 h, followed by addition of 1 volume of protein lysis buffer [10 mM of Tris–HCl (pH 8.0), 1 mM of EDTA, 31 nM of proteinase K, 0.9 μg/ml of glycogen] and incubation at 37°C for 2 h. DNA was recovered from the mixture by phenol extraction, followed by a treatment with 50 μl of RNase A solution (33 ng/ml) at 37°C for 2 h

and by column purification (Qiagen). Input DNA, sampled after sonication, was also de-cross-linked and purified as aforementioned. Finally, all ChIP samples were amplified by whole-genome amplification using the WGA-2 Kit (Sigma-Aldrich) following the manufacturer's instructions for ChIP-chip samples in which the heat-induced fragmentation step is omitted. Mock immunoprecipitations were performed with a BcII β-lactamase-specific nanobody® (here referred to as NbX) (38).

For the spiking immunoprecipitation experiment, covalently cross-linked Ss-LrpB–DNA complexes were prepared as follows: formaldehyde was added (1%, final concentration) to a mixture of 7.7 pM of pUC18p/oSs-lrpB plasmid DNA (31) and 1.5 nM Ss-LrpB protein, and it was incubated at room temperature for 10 min. The reaction was then quenched by adding glycine (final concentration 125 mM) and by incubating for 5 min at 37°C. The mixture was sonicated as previously described. For all ChIP samples, enrichment was evaluated by qPCR relative to input DNA.

Microarray design and data analysis

For DNA microarray analysis, a custom 385 K high-density tiling array was designed and manufactured by NimbleGen™ (Madison, WI, USA; www.nimblegen.com). The probes (50–75 bases, with an average tiling interval of 14 bases) were designed based on the *S. solfataricus* P2 genome sequence (42). Each probe occurred twice on each array. Sample labelling, hybridization and array processing were performed at NimbleGen™. The ChIP input and output samples were labelled with Cy3 and Cy5, respectively. The Ringo package (43) was applied to analyse the raw data sets, including removal of unreliable signals, normalization and smoothing of the data and assignment of ChIP-enriched regions (chers). Venn diagrams were generated using ChIPpeakAnno (44). All microarray data are available in Supplementary Material.

Quantitative real-time PCR

qPCR reactions were performed with a My-iQ™ Single Colour Real-time PCR system (Bio-Rad). Amplification and detection were achieved using SYBR Green Master Mix (Bio-Rad). Each 25 μl of PCR reaction contained ~10 ng of template DNA and 200 nM of each primer. Cycling conditions (10 min at 94°C and 40 cycles of 30 s at 94°C, 30 s at 60°C) were followed by melt curve analysis. Amplicon sizes were between 100 and 250 bp; all primers are listed in Supplementary Table S1. Quantification cycles (Cq) were determined by My-iQ software (Bio-Rad), and relative quantitative analysis was done using the $2^{-\Delta\Delta Ct}$ method (45). All measurements were normalized to reference DNA, a non-related sequence fragment amplified by PCR from *E. coli* gDNA, and spiked at 30 ng/sample before sonication. Experiments were performed at least in duplicate.

RESULTS

Generation, affinity determination and epitope mapping of Ss-LrpB-specific nanobodies®

An alpaca was immunized by six injections at weekly intervals, each time with 200 μg of purified full-length recombinant Ss-LrpB. The plasma obtained 4 days after the last injection showed an end-titre of $\sim 10^5$ [the plasma dilution which still gives an antigen-specific enzyme-linked immunosorbent assay (ELISA) signal, which is ≥3-fold above background]. Subsequently, an immune VHH library comprising $\sim 10^8$ independent transformants was constructed from the peripheral blood lymphocytes taken from the immunized animal 4 days after the last immunization. The library was subjected to two distinct bio-panning experiments, against either full-length Ss-LrpB or the C-terminal domain of Ss-LrpB ('Ss-LrpB C-Term') (36). We included the selection against Ss-LrpB C-Term because the N-terminal domain of Lrp-like transcription regulators contains the DNA-binding helix-turn-helix motif. By selecting binders that recognize epitopes located in the C-terminal oligomerization and effector binding domain, we aimed to increase the chances of obtaining nanobodies® interacting with regions of the regulator that remain accessible on DNA binding. After three rounds of selection, >200 clones were randomly chosen to assess their nanobody® to recognize Ss-LrpB in an ELISA. The nanobody® nucleotide sequence of 75 ELISA positive clones (19 and 56 clones from panning against full-length Ss-LrpB and Ss-LrpB C-Term, respectively) was determined, resulting in 47 different genes (10 and 37 against full-length Ss-LrpB and Ss-LrpB C-Term, respectively), encoding proteins that differ from each other in at least 1 amino acid. Several of the nanobody® sequences possess a nearly identical CDR3 (the third hypervariable antigen-binding loop). Of these binders, it is known that they interact with the same epitope, although sequence differences in other antigen-binding loops (CDR1 and CDR2) might affect the affinity for the antigen (46). Remarkably, 24 different CDR3 sequences could be discerned for the Ss-LrpB C-Term target, and only two different CDR3 sequences were obtained for the full-length target. Twelve nanobody® genes (2 for the full-length and 10 for the C-Term) were re-cloned in an expression vector in fusion with a His_6 tag, expressed and the recombinant protein purified to homogeneity to determine the affinity and to identify binders that recognize a unique epitope by both, surface plasmon resonance (SPR) and ELISA. Based on these criteria, it was decided to continue with three nanobodies®, designated Nb1, Nb11 and Nb9 (Figure 1A). The first two nanobodies® originated from
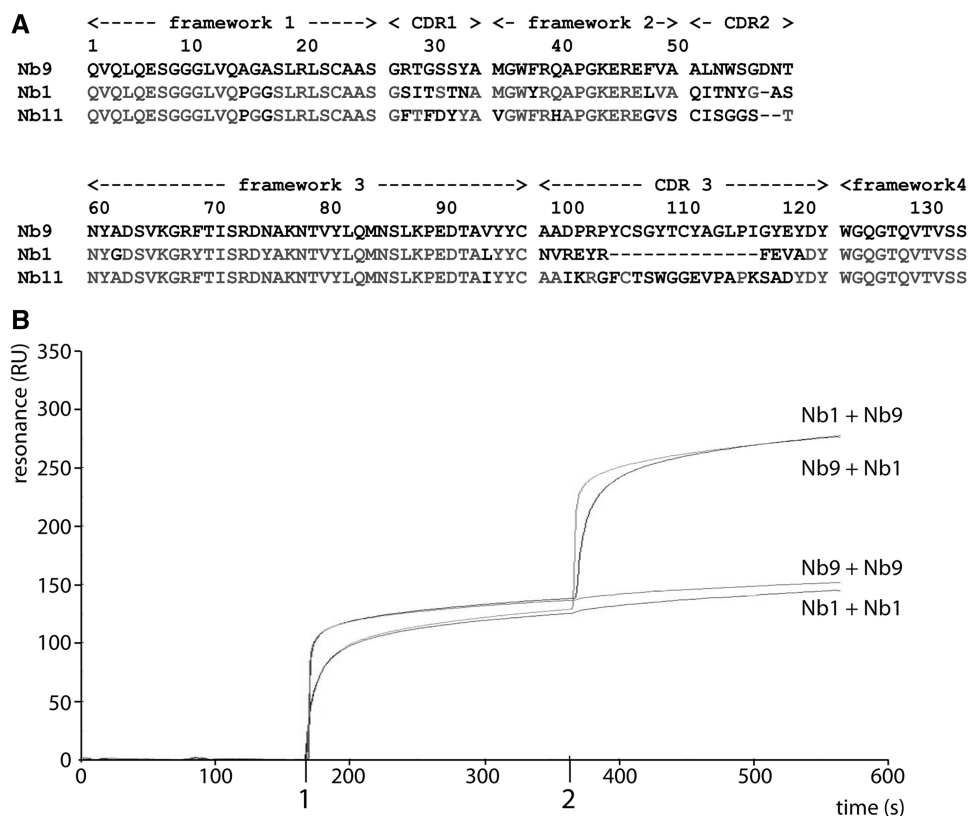

Figure 1. Sequences and epitope analysis of Ss-LrpB-specific nanobodies®. (**A**) Amino acid sequences of Nb1, Nb9 and Nb11. Sequence positions are numbered sequentially, with respect to the Nb9 sequence. Amino acid positions of the framework region and of the three antigen-binding loops (CDR1, CDR2 and CDR3) are indicated on top. (**B**) SPR sensorgram demonstrating the interaction of two nanobodies®, Nb1 and Nb9, with immobilized Ss-LrpB. The nanobody® preparation(s) injected are indicated (1 and 2) on the time axis. The nanobody® preparation(s) injected are indicated above the sensorgram (first nanobody®/second nanobody®).

the pannings on the full-length Ss-LrpB, the Nb9 was retrieved from the C-Term selections. The affinity (K_D) as obtained from SPR ranged from 40 (Nb11) to 1 nM (Nb9) (Table 1). The high affinity of Nb9 is attributed to a high association rate constant (k_{on}), which is ~6- and 64-fold higher than the k_{on} of Nb1 and Nb11, respectively (Table 1). The k_{off} rate (~10^{-3} s^{-1}) is similar for all three nanobodies®. Therefore, Nb9 is the best candidate nanobody® for ChIP in terms of affinity. SPR experiments, involving the sequential injection of two nanobodies® at target saturating concentrations on the immobilized Ss-LrpB, further demonstrated that Nb1, Nb11 and Nb9 indeed bind to independent sites on the regulator (Figure 1B). This figure shows that Nb1 and Nb9 bind concomitantly to the immobilized Ss-LrpB protein: a second injection of the same nanobody® did

not result in a significant RU change, indicating saturation of the first occupied epitope. However, a second injection of the counterpart nanobody® resulted in a similar RU change as observed after the first injection. Similar results were obtained for Nb1/Nb11 and Nb9/Nb11 combinations (data not shown). The same epitope grouping whereby the three nanobodies® recognize three independent epitopes on the same antigen was further confirmed by ELISA (data not shown).

Specificity of the Ss-LrpB–nanobody® interaction

Thus far, all interaction analyses were performed with purified immobilized Ss-LrpB and, therefore, do not address the specificity of the nanobodies® for their cognate target in a complex mixture. Moreover, immobilization of antigen can lead to (partial) denaturation, thereby exposing epitopes that are not present or accessible in the native soluble protein. To evaluate the capacity of nanobodies® to capture Ss-LrpB in solution and to provide further information on their specificity, we performed pull-down assays with the three selected nanobodies®, using total protein extracts from *E. coli* cells expressing recombinant Ss-LrpB (Figure 2A). It is clear that different amounts of Nb1 (from 6.5 to 25 μg) capture specifically Ss-LrpB from

Table 1. Binding parameters of Ss-LrpB-specific nanobodies® on immobilized Ss-LrpB, as determined by SPR

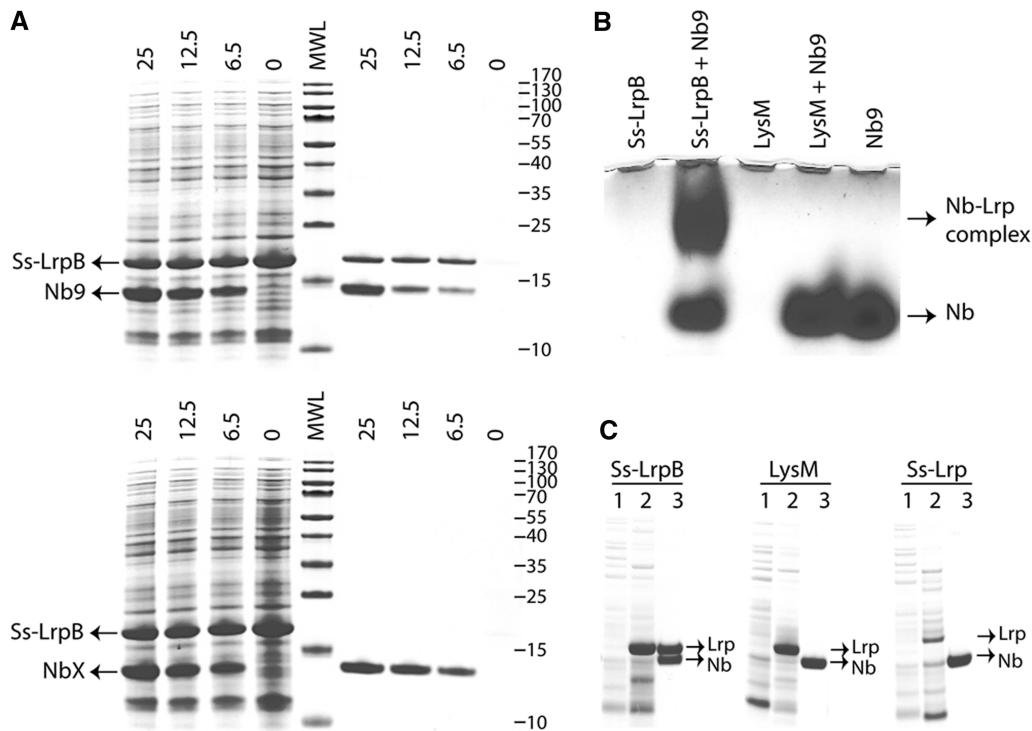| Nanobody®	k_{on} (M^{-1}s^{-1})	k_{off} (s^{-1})	K_D (M)
Nb1	2.84×10^5	1.2×10^{-3}	4.34×10^{-9}
Nb9	1.79×10^6	1.8×10^{-3}	1.03×10^{-9}
Nb11	2.8×10^4	1.1×10^{-3}	3.92×10^{-8}

Figure 2. Specificity analysis of nanobodies® directed against Ss-LrpB. (**A**) SDS–PAGE analysis of pull-down assays with *E. coli* cell extracts with overexpressed Ss-LrpB. The amount of His$_6$-tagged nanobody® (in μg) added to the cell extract before immunocapturing with Ni^{2+}-loaded magnetic beads is indicated on top of the SDS–PAGE. The extracts before and after immunocapturing are shown to the left and right of the molecular weight ladder (MWL), respectively. Protein molecular masses are indicated in kDa. The top panel shows the pull-down assay with Nb1 and the bottom panel with NbX (a control nanobody® raised against BcII β-lactamase). Positions of migration of Ss-LrpB and nanobody® is indicated on the left. (**B**) Native protein gel electrophoresis of nanobodies® and Lrp-like proteins. The identity of the proteins, and the position of the nanobody® or its complex (arrows) are shown. (**C**) SDS–PAGE analysis of pull-down assays with *E. coli* cell extracts with overexpressed paralogues Ss-LrpB, Ss-LysM or Ss-Lrp, as indicated. For Ss-Lrp, additional purified protein was added to the cell extract. Lane 1 corresponds to *E. coli* extracts of cells containing the expression plasmid pET24a without insert (negative control), lane 2 corresponds to the cell extracts with the Lrp protein expressed from recombinant pET24a vector and lane 3 corresponds to the sample shown in lane 2 after pull-down with Nb9.
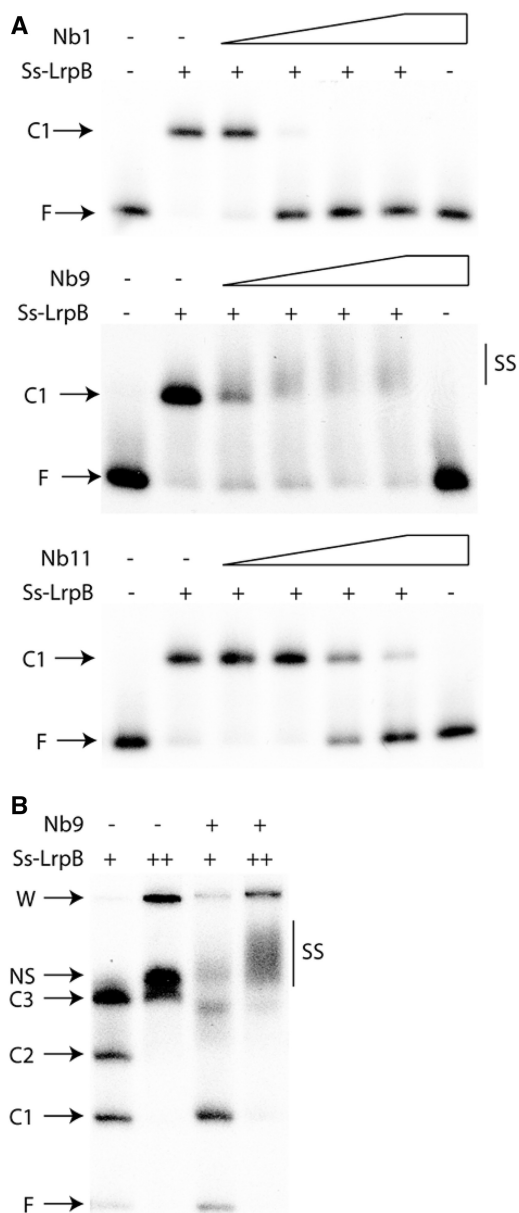
Figure 3. EMSA analysis of the interaction of the nanobodies® with DNA-bound Ss-LrpB. (**A**) EMSAs of Ss-LrpB binding and effects of supplementary addition of an Ss-LrpB-specific nanobody® to a ^{32}P-labelled 182-bp DNA fragment, containing a single binding site [Box1 of the *Ss-lrpB* control region (31)]. The nanobody® used (Nb1, Nb9 or Nb11) is indicated next to each autoradiograph. The final molar concentration of Ss-LrpB monomer added to the reaction mixture is 80 nM, whereas the concentration of the nanobodies® is 80, 160, 800 and 1600 nM, respectively. The last lane contains 1600 nM of nanobody® and free DNA, but no SsLrpB. The positions of migration of the free DNA (F) and the protein–DNA complex (C1) are indicated at the left of the autoradiograph. Supershifting of the complex is denoted with 'SS' at the right end of the autoradiograph. (**B**) EMSA of Ss-LrpB binding and effects of supplementary addition of Nb9 to a ^{32}P-labelled 185 bp-DNA fragment containing the three binding sites of the *Ss-lrpB* control region. The final monomer concentrations of Ss-LrpB are 90(+) and 270 nM (++), respectively; the final concentration of Nb9 added to the mixture is 500 nM. The positions of the free DNA (F), three complexes (C1, C2 and C3), super-shifting caused by nanobody® binding (SS) and the wells (W) are indicated. Besides the formation of the three specific complexes, non-specific binding (annotated as NS) is observed on adding high amounts of Ss-LrpB; the relative mobility of the NS band is highly variable and dependent on the protein concentration.

crude cell extract, and that *E. coli* endogenous proteins are not observed after pull-down. Similar results were obtained in pull-down assays with Nb9 and Nb11 (data not shown). The control nanobody®, NbX with specificity for an antigen that is not expressed by *E. coli*, fails to capture Ss-LrpB or any other protein, thereby demonstrating its suitability as a negative control in ChIP (Figure 2A, lower panel).

However, the lack of cross-reactive antigens in *E. coli* does not guarantee that proteins displaying homology with Ss-LrpB are absent in *S. solfataricus*. In particular, *S. solfataricus* Lrp family members, other than Ss-LrpB, may cross-react with Ss-LrpB-specific nanobodies®. Two such Lrp family members, Ss-Lrp (encoded by *Sso0606*) and LysM (encoded by *Sso0157*), have already been reported to exhibit 31 and 25% sequence identity and 60 and 52% sequence homology to Ss-LrpB, respectively (32,47). In addition, these Lrp-like transcription factors exhibit large structural homologies (33). Nevertheless, physical interactions between Nb9 and LysM could be excluded from the results of a native protein PAGE with mixtures of the two proteins (Figure 2B). The Lrp-like regulators migrate out of the gel towards the cathode because of their high-isoelectric point, whereas the nanobodies® migrate into the gel because of their overall negative charge at pH 8.5. Complexes between Lrp proteins and nanobodies® enter into the gel, but with a slower migration velocity than the nanobodies® alone. Nb9 forms a stable complex with Ss-LrpB, whereas this type of complex is not observed with LysM (Figure 2B). Pull-down assays with total protein extracts from *E. coli* cells overexpressing Ss-Lrp or LysM further demonstrate the inability of Nb9 to capture these proteins (Figure 2C). Similar results were obtained with Nb1 and Nb11 (data not shown).

Interaction between nanobodies® and DNA-bound Ss-LrpB

DNA binding might influence the interaction between antibody and transcription factor because of epitope masking and/or conformational changes. Here, we used EMSAs (Figure 3) to investigate the possible occurrence of supershifts as readout for nanobodies® associating *in vitro* with Ss-LrpB in complex with its cognate target DNA, and as an indicator for the suitability of nanobodies® for ChIP. Using a DNA fragment containing a single binding site for SsLrpB, stable complexes are formed, in which the semi-palindromic binding site is bound by an Ss-LrpB dimer (Figure 3A). It is shown that the nanobodies® do not provoke a band shift of the free DNA in an EMSA (last lane). However, the addition of Nb1 or Nb11 to pre-equilibrated Ss-LrpB–DNA complexes shifts the protein–DNA equilibrium towards dissociation of the preformed complexes. The Nb1 induced dissociation occurs at lower nanobody® concentration than with Nb11, indicating that the dissociation is proportional to the affinity of the nanobody®–Ss-LrpB interaction. This dissociation can be explained as resulting either from a direct association of the nanobody® with the DNA-binding face of

the Ss-LrpB, so that the nanobody® competes effectively with the DNA for the Ss-LrpB protein, or from a nanobody®-induced conformational change in Ss-LrpB that affects its DNA binding allosterically in a negative fashion. The former explanation would discourage the use of Nb1 and Nb11 in ChIP, as their Ss-LrpB epitopes are probably unavailable in cross-linked nucleoprotein.

Conversely, Nb9, with specificity to the C-terminal domain of Ss-LrpB, binds to the Ss-LrpB–DNA complex as evidenced by supershifting (Figure 3A, middle panel). This suggests that Nb9 recognizes an epitope that is not directly involved in, or affected by, DNA binding. Therefore, Nb9 is definitely the best candidate for ChIP.

Ss-LrpB interacts with its main DNA targets (control region of own gene and of the neighbouring pyruvate ferredoxin oxidoreductase (*porDAB*) operon) by binding cooperatively to three regularly spaced semi-palindromic binding sites (31,34). On binding, all three sites of the *Ss-lrpB* control region, the three protein dimers closely interact and are assumed to wrap the DNA, causing large conformational changes with respect to the nucleoprotein complex with a single binding site (35). Besides the formation of three specific complexes, non-specific binding is observed on adding larger amounts of Ss-LrpB, visible as a complex (annotated 'NS') of variable relative mobility in gel and dependent on the protein concentration (31). To analyse Nb9 interaction with nucleoprotein complexes involving three Ss-LrpB binding sites, which are expected to be prevalent *in vivo*, an EMSA was performed with a tripartite operator-containing DNA fragment (Figure 3B). At the highest Ss-LrpB concentration used, the addition of Nb9 causes supershifting and the disappearance of the triple bound Ss-LrpB–DNA complex (C3), indicating the recognition of these complexes by Nb9. At the lowest Ss-LrpB concentration used, with all three distinct complexes (C1, C2 and C3) being present, Nb9 interacts only with complexes having two and three Ss-LrpB dimers bound (C2 and C3). These data, in conjuncture with those presented in Figure 3A (middle panel), suggest that although Nb9 binds all three complexes, it preferentially interacts with complexes involving two and three Ss-LrpB dimers.

Optimization of the nanobody®-assisted ChIP assay for *S. solfataricus*

Cross-linking conditions
The formaldehyde cross-linking of DNA–protein complexes is a crucial step in ChIP (17). As this process is temperature-dependent and is reversed at high temperatures, it is impossible to perform cross-linking at physiological temperatures of hyperthermophilic organisms. Although formaldehyde-induced fixation of hyperthermophilic archaea chromatin works sufficiently well at room temperature (48,49), we performed formaldehyde cross-linking at 37°C which is, as compared with room temperature, closer to hyperthermophiles' physiological temperature.

Cross-linking time is also an important parameter: a time that is too short might lead to insufficient cross-linking, and as a consequence to inability to detect an interaction, whereas excessive cross-linking might lead to epitope unavailability because of epitope masking or aggregation (11,17,50). To optimize the cross-linking time, we performed a time-course experiment in which the efficiency of cross-linking was evaluated by separating cross-linked from non–cross-linked DNA with phenol extraction followed either by gel electrophoresis analysis (see Supplementary Figure S1) or by qPCR quantification of SsLrpB-target and non-target genomic regions (Figure 4A). For all genomic regions tested, of which two are shown in Figure 4A, the fraction of protein–cross-linked DNA (over total DNA) reached values between 84 and 99% after 1 min cross-linking. Moreover, these values did not change significantly on increasing the cross-linking time. Cross-linking efficiencies varied somewhat depending on the genomic region, which can be explained by differences in the abundance of genome-associated proteins (51).

In conclusion, formaldehyde treatment for 1 min at 37°C is sufficient to cross-link *S. solfataricus* chromatin. This time is considerably shorter than the cross-linking time reported previously in eukaryotic or bacterial ChIP protocols, which varies from 10 min to several hours (7,50,52). Note that we analysed cross-linking globally while individual proteins can have varying cross-linking efficiencies. To ensure successful cross-linking of Ss-LrpB, we decided to perform the cross-linking for 5 min for all further experiments.

Sonication conditions
Sonication, to fragment the DNA in appropriate sizes and to solubilize the chromatin, is one of the most variable and critical steps in ChIP, and optimal conditions depend on cell type, cell quantity, chromatin structure and so forth (5). Insufficient sonication might lead to loss of resolution of binding events, whereas over-sonication can result in the disruption of cross-linked protein–DNA complexes and introduction of noise in the microarray data.

To determine the optimal sonication conditions, we performed small-scale tests for different periods of time ranging from 3 to 30 min and analysed both fragment size distribution and dissociation of protein–DNA complexes (Figure 4B and C). Sonication for 6, 9 and 18 min yielded similar results with DNA size distribution of ∼0.2–0.6 kb. On longer sonication (18 min), cross-linked protein–DNA complexes tend to dissociate (Figure 4C). The extent of dissociation was somewhat variable, depending on the genomic region under study.

To ensure both the stability of cross-linked protein–DNA complexes and an optimal fragment size distribution, we chose to sonicate for 9 min in further experiments.

Minimal amount of cells
The number of cells subjected to ChIP is also an important element for a successful assay. It needs to be sufficiently high to obtain robust results (5), whereas it also affects the concentration of targets, so that in
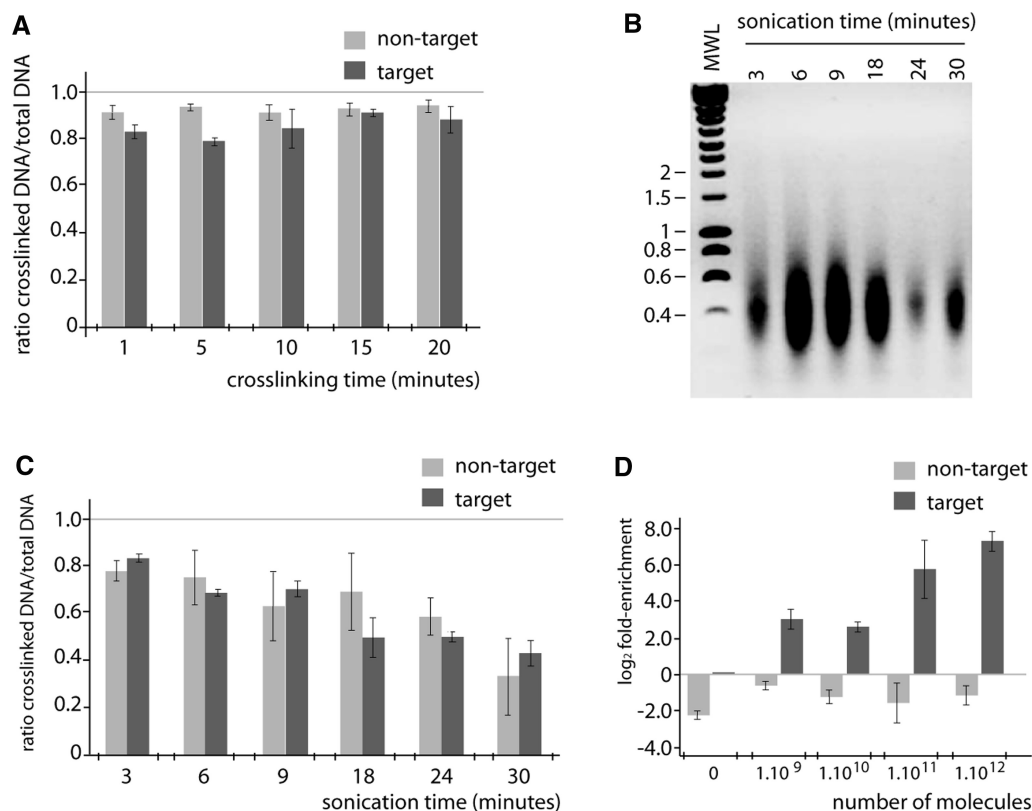
Figure 4. Optimization of different experimental steps in the ChIP procedure. (**A**) qPCR data of small-scale formaldehyde cross-linking tests showing the degree of cross-linking as a function of time. 'Non-target' indicates a genomic region that is not bound by Ss-LrpB (*Sso0720* ORF), and 'target' indicates a genomic region that is bound by Ss-LrpB (control region of *Ss-lrpB*); PCR primer sequences are given in Supplementary Material (Supplementary Table S1). Error bars represent standard deviations. (**B**) Small-scale tests of the effect of sonication time on the DNA fragment size. Cells were first cross-linked at 37°C for 5 min and then subjected to sonication for different amounts of time. The lengths of de-cross-linked and sonicated DNA were analysed by agarose gel electrophoresis. MWL represents molecular weight ladder, with the sizes of relevant bands in kb. (**C**) qPCR data of small-scale sonication tests showing the fraction of cross-linked complexes as a function of time. (**D**) qPCR data of small-scale chromatin immunoprecipitation tests with different amounts of added cross-linked Ss-LrpB–DNA complexes, as indicated along the *x*-axis. Data are given as the $\log_2$ values of the ratio ChIP output DNA/input DNA.

combination with the antibody affinity (and specificity) it might influence the outcome as well.

Cell counting by plating and by microscopy indicated a cell density of 2×10^7 cells/ml for a cell suspension with $OD_{600\,nm}$ of 0.5 (exponential growth phase; data not shown). Taking into account that *S. solfataricus* is a haploid species characterized by a long G_2 cell cycle phase (53,54), most cells are expected to have two chromosomal copies, and a 50 ml culture at an $OD_{600\,nm}$ of 0.5 is expected to harbour ~ 1–2×10^9 copies of each genomic binding site.

To determine the minimal amount of cells required for ChIP-based DNA enrichment with Ss-LrpB-specific nanobodies®, a preliminary immunoprecipitation assay was performed with Nb9 (Figure 4D). Here, different amounts of *in vitro* prepared cross-linked Ss-LrpB–DNA complexes, containing the *Ss-lrpB* operator, were added to a constant amount of cross-linked *S. solfataricus* cells. The mixture was subjected to ChIP by Nb9. The enrichment of the *Ss-lrpB* operator, compared with input DNA and normalized to *E. coli* reference DNA that was added to all samples before sonication, in the immunoprecipitated DNA was analysed by qPCR. Likewise, an unrelated

genomic region, not bound by Ss-LrpB, was analysed as negative control. No ChIP enrichment was observed using cells from 50 ml culture (Figure 4D). In contrast, after spiking, the samples with different amounts of cross-linked Ss-LrpB–DNA complexes, enrichments exceeding a 4-fold ratio ($\log_2$ value of 2), were observed. Parallel ChIP with control nanobody® NbX showed no enrichment (data not shown). These experiments suggest that at least 2–3×10^9 specific complexes need to be present for detection by qPCR. Based on this result, 200 ml cultures, corresponding to $\sim 4 \times 10^9$ cells, were used in subsequent ChIP-chip experiments.

Comparative analysis of ChIP performance of nanobodies® using predefined DNA targets

Although Nb9 is the most promising nanobody® for ChIP in terms of affinity and epitope location, we compared the performance of the three Ss-LrpB-specific nanobodies® by evaluating nanobody®-mediated enrichment of known Ss-LrpB binding sites by qPCR and ChIP-chip. To avoid variability introduced by ChIP, the same ChIP DNA was used for both qPCR and ChIP-chip. In the first approach, enrichment of known target regions was
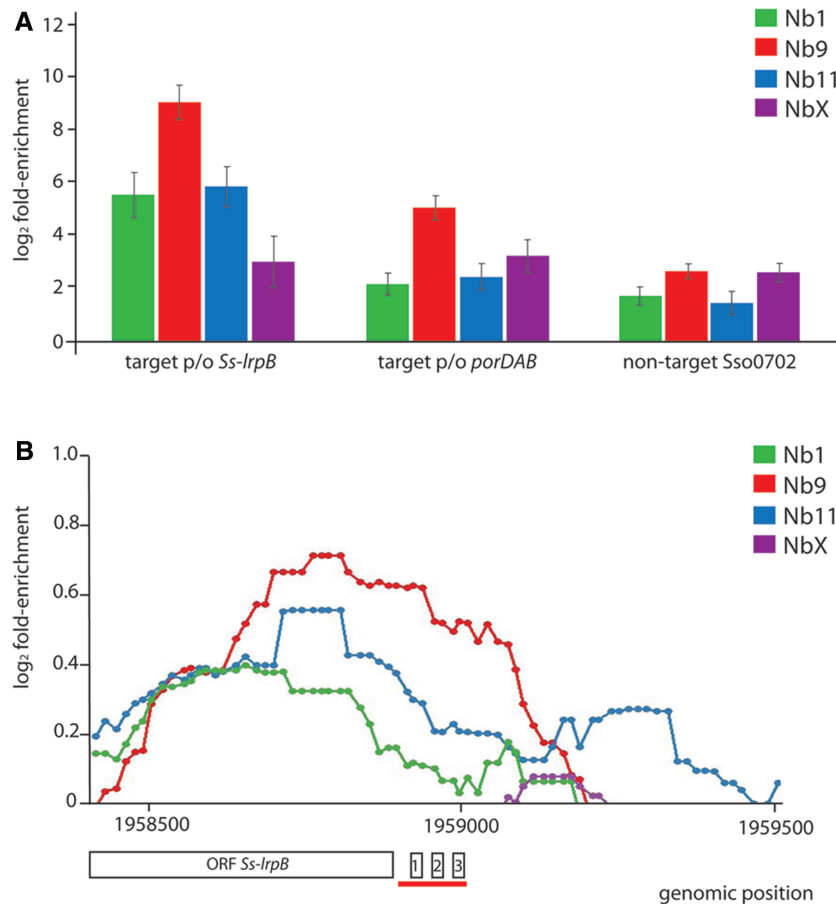
Figure 5. Nanobody®-assisted ChIP enrichment of predefined targets. (**A**) qPCR analysis of ChIP samples, prepared using different nanobodies® for immunoprecipitation (Nb1, Nb9, Nb11 and NbX). Identical samples were used for this analysis (after amplification) and microarray analysis. Data are expressed as $\log_2$ values of the fold-enrichment ratio ChIP output DNA/input DNA. Error bars correspond to standard deviations. The analysis has been performed for three genomic regions; PCR primer sequences are given in Supplementary Material (Supplementary Table S1). (**B**) Zoomed view of raw ChIP-chip signals (Cy5/Cy3 ratio) for all probes in the genomic region harbouring a high-affinity Ss-LrpB target, which is the control region of the *Ss-lrpB* gene itself. Data are given as $\log_2$ values of the enrichment ratio ChIP output DNA/input DNA for the ChIP-chip assays performed with samples enriched using Nb1, Nb9, Nb11 or NbX, as colour-coded. The indicated genomic positions correspond to those in the published genome sequence (42). The position of the *Ss-lrpB* ORF is indicated at the bottom (encoded on the reverse complementary strand with respect to the published genome sequence). The three characterized Ss-LrpB binding sites are schematically indicated as well, with 1, 2 and 3 denoting Box1, Box2 and Box3, respectively (31). The red horizontal bar corresponds to the genomic sequence that was amplified in the qPCR experiment.

analysed as the evaluation criterion (Figure 5). A non-target genomic region and mock immunoprecipitation with the nanobody® NbX were used as negative controls. By using qPCR as readout, significant enrichment was observed with negative controls in ChIP DNA, as compared with the input DNA ($\log_2$ values between 1 and 3). Although the whole-genome amplification protocol might result in a minimal amplification bias (16), we observed a bias towards more efficient amplification of longer DNA molecules (data not shown), probably because longer DNA fragments might anneal to more primers yielding a larger number of amplification products. This bias possibly explains the observed background enrichment, as the molecular weight of the reference *E. coli* DNA is significantly lower than the average molecular weight of the chromatin DNA. Therefore, amplification could cause a higher ratio of chromatin DNA/reference DNA in the ChIP DNA as compared with the unamplified input DNA, irrespective

of immuno-enrichment (Figure 5A). Nevertheless, this bias does not affect the assessment of the ChIP enrichments, as they were calculated based on the relative fold enrichment and were compared with the ChIP enrichment of the negative control NbX. The experiment with the Nb9 resulted in ∼500- and 33-fold enrichment of the *Ss-lrpB* and *porDAB* operators DNAs, respectively (Figure 5A). This difference might reflect the difference in the binding affinities of Ss-LrpB for the two operators. The use of Nb1 and Nb11 enriched the target *Ss-lrpB* operator ∼47- and 62-fold, respectively. Furthermore, the Nb1 and Nb11 enrichment of *porDAB* operator DNA failed to exceed the background levels. Next, genome-wide ChIP-chip experiments were performed with DNA prepared with each of the nanobodies®, and raw $\log_2$ fold-enrichment values were compared for the genomic regions known to bind Ss-LrpB (Figure 5B). Although the sensitivity of this assay is lower than qPCR, the trends of the peaks confirm the
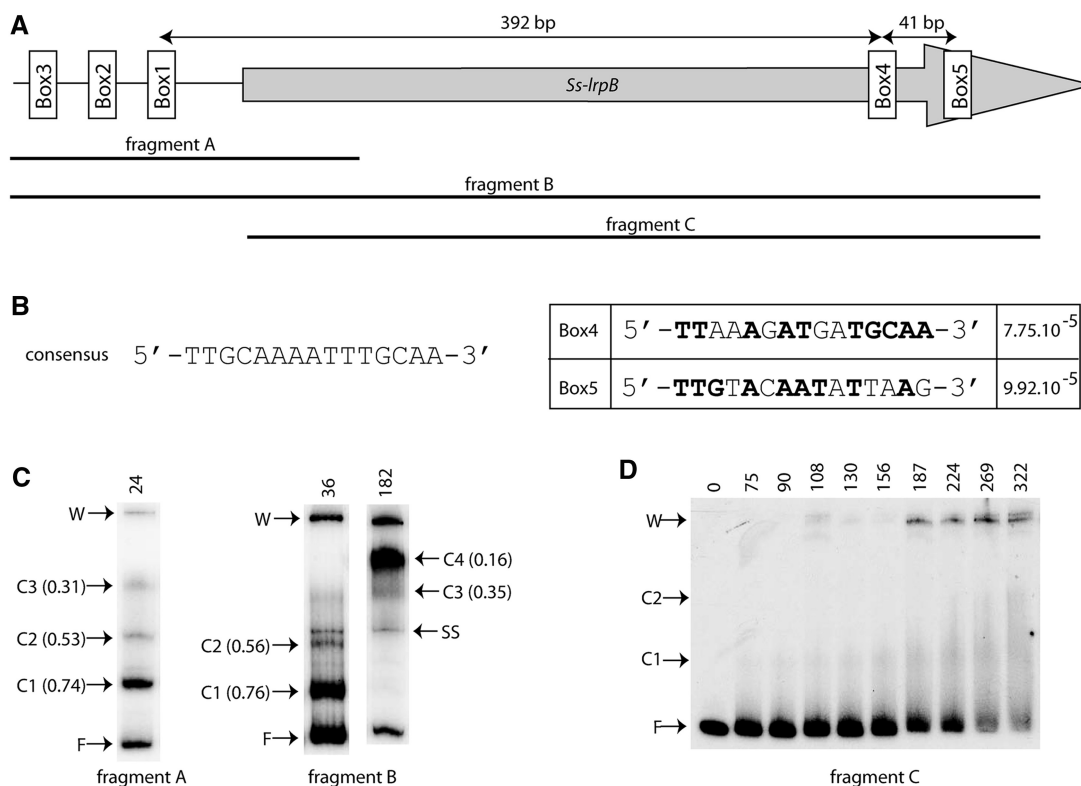
Figure 6. Binding of Ss-LrpB to additional operators in the *Ss-lrpB* ORF. (**A**) Schematic overview of the locations of Ss-LrpB 15-bp-long binding motifs (white rectangles) in both the control and the coding regions, depicted by a line and a grey shaded arrow, respectively. The regions that are spanned by the different fragments tested in EMSAs are indicated below. (**B**) Sequences of the newly identified Ss-LrpB binding motifs, Box4 and Box5 (right side), identified by applying MEME SUITE (55) using all previously identified binding sites (31,34). Next to the sequences, *P*-values are given. Residues that correspond to the Ss-LrpB consensus, which is shown to the left, are shown in bold. (**C**) EMSAs of the binding of Ss-LrpB to fragments A and B, as indicated. On top, the applied Ss-LrpB monomer concentration is indicated (in nM). The positions of free DNA (F), specific protein–DNA complexes (C1–C4), single-stranded DNA (SS) and the wells of the PAG are indicated. In brackets, relative mobility of the different complexes is given. The mobility was calculated by dividing the distance of migration of a band corresponding to a complex with the distance of migration of the band corresponding to free DNA (both measured with respect to the bottom of the well). (**D**) EMSA of the binding of Ss-LrpB to fragment C, encompassing the ORF. Ss-LrpB monomer concentrations (in nM) are indicated above the autoradiograph, and the positions of free DNA (F), complexes (C1, C2) and the wells (W) are indicated.

relative enrichment ratios observed with qPCR. For the *porDAB* operator region, absolute $\log_2$ values were somewhat higher, but the ChIP curve obtained with control nanobody® NbX coincided with those of Nb1 and Nb11 (data not shown).

The ChIP-chip derived binding peaks for the known autoregulatory binding sites exhibit an unexpected shape, centred over the coding part of the gene rather than over the operator region (Figure 5B). This observation prompted us to re-investigate autoregulatory binding of Ss-LrpB, and indeed, two additional potential binding sites were predicted *in silico* in the open reading frame (ORF) sequence (Figure 6A). These sites, tentatively called Box4 and Box5, are located at the 3′-end of the ORF with a spacing of 26 bp. Based on sequence similarity with the Ss-LrpB consensus sequence (56), both sites are expected to be low-affinity sites (Figure 6B).

To further investigate possible Ss-LrpB binding within the ORF, EMSAs were performed with a fragment encompassing the promoter region only, both the promoter region and the coding region and with a fragment spanning the coding region only (Figure 6C

and D). In the former case, three complexes (C1–C3) are formed, whereas a fourth complex (C4) that migrates slower than the other three complexes (C1–C3) is clearly present when the DNA fragment comprises both the promoter and the ORF. In contrast to Ss-LrpB complexes with the fragment containing the promoter region-only, the presence of the third complex (C3) is seriously reduced, obviously in favour of forming a new complex, C4. This suggests a cooperative binding to additional binding sites within the ORF. Supplementary DNA deformations (looping) and a higher protein stoichiometry may explain the significant reduction in the relative mobility of complex C4. Furthermore, low-affinity binding to the ORF fragment is inferred (Figure 6D), as two nucleoprotein complexes are detected in these EMSA (C1 and C2), although they result in smearing, reflecting binding instability. In conjunction, we provide strong evidence both *in vivo* and *in vitro* that Ss-LrpB binds two additional binding sites in the *Ss-lrpB* ORF, located 392 bp downstream of Box1 and oriented on the same side of the DNA helix (with a centre-to-centre distance of four helical turns).

Thus far we analysed the ChIP enrichment of two high-affinity Ss-LrpB targets. Two other known Ss-LrpB targets, the operator regions of *Sso2126* and *Sso2127*, bind Ss-LrpB at a single site *in vitro* (34), and Ss-LrpB indeed exerts a weak activation effect on gene expression of these targets. After inspection of the ChIP-chip binding profiles, recorded in the growth conditions in which the expression of *Sso2126* and *Sso2127* genes was analysed, none of the nanobodies® enriched these sequences. Given the weak regulatory effect of Ss-LrpB on these targets under the growth conditions used, the Ss-LrpB binding affinity for these sequences might be low, or the Ss-LrpB is only binding to these recognition sites in a sub-population of cells, possibly because of the effect of cofactors.

Comparative analysis of ChIP performance of nanobodies® using genome-wide data

In an alternative approach, genome-wide ChIP-chip binding profiles were evaluated to assess the performance of different nanobodies® (Figure 7). Binding patterns obtained with Nb1 and Nb11 almost completely overlap with the patterns obtained with control NbX and, consequently, fail to reveal any novel potential Ss-LrpB binding sites (Figure 7A, first and third panel). The two sites identified by Nb11 at cut-off of 1.0 and the site identified both by Nb11 and Nb1 at cut-off of 0.8 (Figure 7B) are considered as false-positive sites because the $\log_2$ enrichment of the negative control NbX corresponding to these sites are 0.93, 0.82 and 0.79, respectively. The mean $\log_2$ enrichment over the whole genome by NbX is 0.22. In contrast, the binding profile obtained with Nb9 showed significant novel Ss-LrpB binding regions throughout the entire genome, besides the previously known Ss-LrpB target sites (Figure 7A, middle panel). Depending on the significance threshold, ChIP-chip analysis using Nb9 revealed between 36 (cut-off = 2-fold or 1.0 $\log_2$-fold enrichment) and 181 (cut-off = 1.5-fold or 0.6 $\log_2$-fold enrichment) novel putative Ss-LrpB binding sites (Figure 7B).

The ChIP-chip signals of most of the newly discovered potential binding sites, called ChIP-enriched regions (chers), were higher than that of the *Ss-lrpB* operator region. To further validate the validity of these chers to represent genuine novel Ss-LrpB genomic association sites, qPCR analysis was performed for a selection of 13 chers that scored a $\log_2$ ChIP-chip value between 1.0 and 2.0 (Figure 8). All these chers showed enrichment in qPCR, and for more than half of them, enrichment values far exceeded the background enrichment level. Therefore, the use of Nb9 leads to the discovery of novel potential targets with ChIP-chip, whereas the use of Nb1 and Nb11 does not, although qPCR analysis shows enrichment of the main target (*p/o Ss-lrpB*) by these latter Nbs (Figure 5A). A statistically solid identification and further analysis of novel Ss-LrpB targets in the context of the physiological function of the transcription factor is beyond the scope of this work and will be published elsewhere.

DISCUSSION

Chromatin immunoprecipitation is a valuable technique, especially in combination with deep sequencing or microarray analysis to decipher gene regulatory networks. However, its success is largely dependent on the quality of the antibodies (i.e. specificity and affinity for its cognate antigen) (5,11,15,16). Cross-reactivity of the antibody with other non-cognate antigens is an important source of high background signals and false-positive outcomes in genome-wide ChIP assays. A study with antibodies directed against modified histones has demonstrated a high level of specificity problems, as >20% of a panel of tested antibodies, including those with a 'ChIP-grade' label, were shown to fail in ChIP experiments (18). As argued in the 'Introduction' section, recombinant antibodies constitute an interesting and renewable source of monospecific antibodies for various applications including ChIP.

What is the problem with pAbs and mAbs in ChIP? The polyclonal antibody preparations consist of a mixture of different antibodies, each with a different epitope recognition mode. Hence, it can be argued that pAbs are to be preferred over mAbs because of lower incidences of epitope masking in the cross-linked chromatin (17). However, the pAbs are obviously less suitable for ChIP in terms of specificity (18,19), and their use increases the risk of association to non-cognate antigens, thus cross-reaction. Furthermore, the specificity of pAbs varies from batch to batch, necessitating a specificity analysis for each preparation (19). With mAbs, which is renewable antibody source, most of these problems of non-cognate antigen binding can be avoided, and the antibody that performs best in terms of specificity and ChIP-efficiency can be selected and used repeatedly and reproducibly. However, as the mAb recognizes, in principle, only one epitope structure, this epitope may be masked during DNA binding, or within the chromatin architecture when interaction occurs with other transcription factors, or by fixation during cross-linking. The problem of epitope masking can be avoided by careful design of the immunization and antibody selection protocols. For instance, the use of cross-linked DNA–protein complexes to screen the mAbs from hybridomas should yield antibodies with greater chance of success in ChIP. However, this is rarely done. Finally, irrespective of whether polyclonal or monoclonal antibodies are used, antibodies are complex molecules comprising an Fc part that is recognized by multiple effector molecules, and thus forms a possible source of multiple unwanted binding events in ChIP.

The latter complication is expected to be absent with antibody fragments, such as scFv and nanobodies®, which lack the Fc part. Nanobodies® are recombinant single-domain antigen-binding entities derived from unique heavy chain only antibodies naturally occurring in camelids (26). Sharks also possess such heavy chain antibodies, referred to as IgNARs. However, IgNARs are more ancestral antibodies compared with the camel variant (57), and the immunization of sharks might be rather complicated. The immunization of camelids
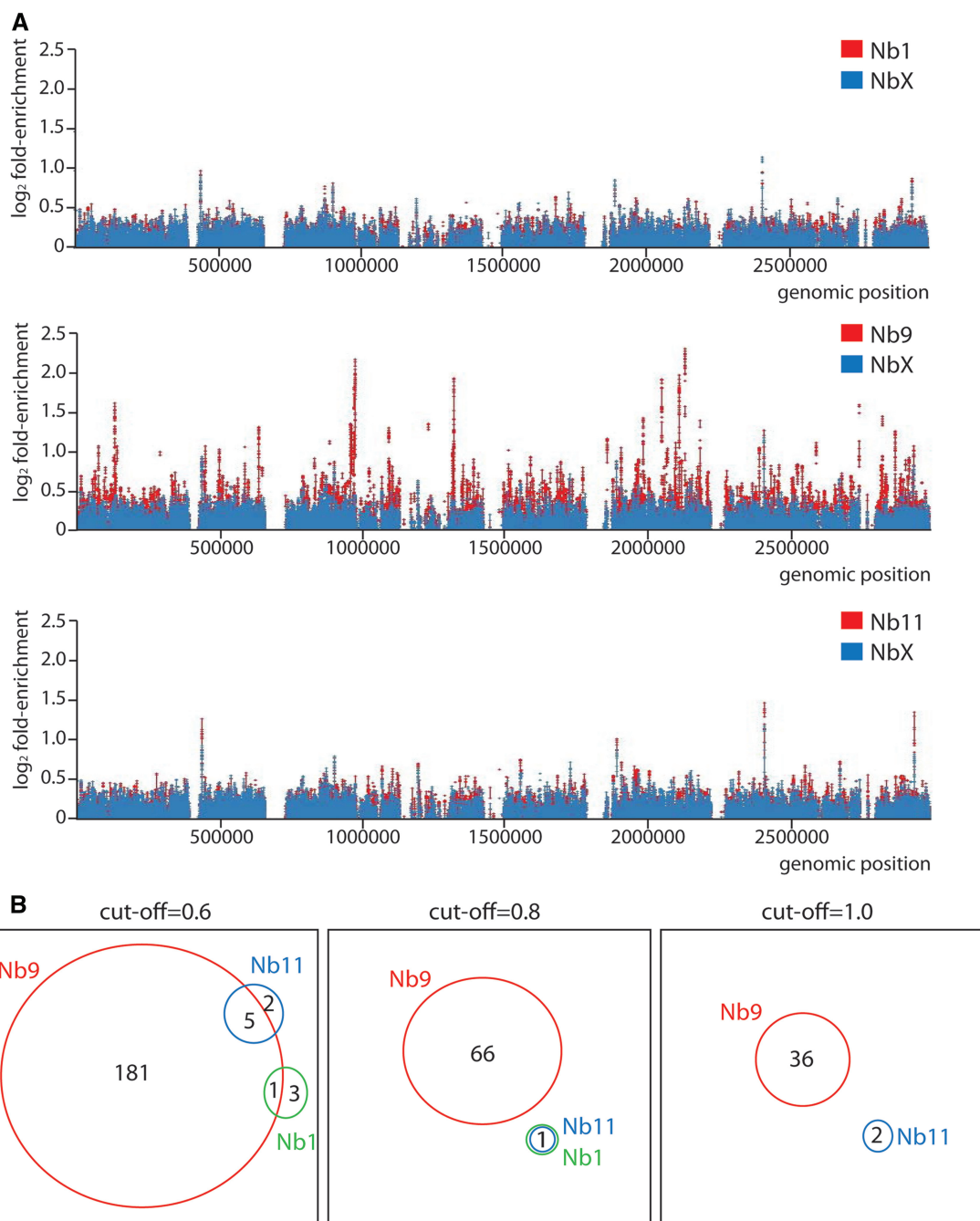
Figure 7. (**A**) Genome-wide ChIP-chip profiles of microarray hybridizations with ChIP samples using Nb1, Nb9 or Nb11, as indicated. Data were analysed, normalized and smoothed as described in 'Materials and Methods' section. The genome coordinates (in bp) are given on the *x*-axis, whereas the *y*-axis represents $\log_2$ values of the enrichment ratio ChIP output DNA/input DNA. The profiles of the immunoprecipitation assays with any of the Ss-LrpB-specific nanobodies® (red) are overlaid with the profile of the mock immunoprecipitation with NbX (blue). Some genomic regions lack signal because of an undefined technical bug. (**B**) Venn diagrams schematically displaying the number of ChIP-enriched regions (chers) detected in the data sets obtained with Nb1 (green), Nb9 (red) and Nb11 (blue) and the overlaps between these chers. Different diagrams are shown for different cut-off values expressed in $\log_2$ fold-enrichment. All signals exhibiting a significant overlap with a signal in the NbX data set were disregarded.

(camel, dromedary, alpaca and llama) is more practical: these animals are routinely vaccinated in farms with optimized adjuvants, and we shortened the immunization time to 6 weeks. In addition, the cloning of the nanobody® genes form the peripheral blood B-cells of the immune animal and the subsequent identification of recombinant, antigen-specific nanobodies® after phage display became indeed a fast and straightforward technology (27,30,58). Moreover, nanobodies® are well expressed in microbial systems, and with their small size (<MW 15 000), high robustness and high specificity for their cognate antigen they are versatile. Nanobodies® seem to suffer minimally from non-specific antigen capturing in the context of complex proteomes as illustrated here (Figure 2).
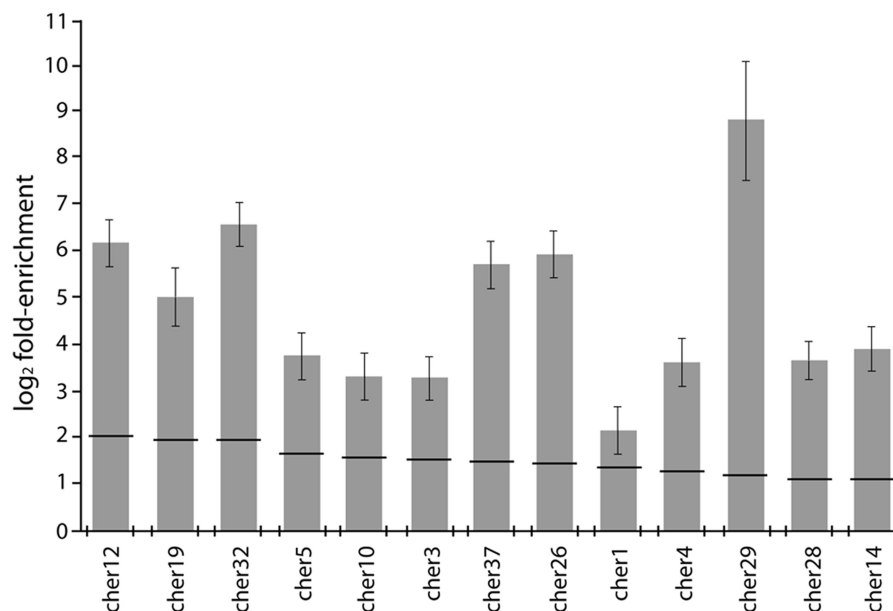
Figure 8. Novel potential Ss-LrpB targets discovered by Nb9-assisted ChIP-chip. Data are given for 13 ChIP-enriched regions (chers) exhibiting the highest signals detected in the ChIP-chip assay ($\log_2$ values between 1.0 and 2.0), ranked in descending order. None of these chers displayed significant signals in the NbX data set. Chers are labelled, and the genomic positions corresponding to their peaks are revealed in Supplementary Material (Supplementary Table S2). qPCR data are shown as grey columns with error bars representing standard deviations. Horizontal bars crossing the columns represent the maximum values detected in the ChIP-chip analysis. All data are given as $\log_2$ values of the enrichment ratio ChIP output DNA/input DNA.

This seems to be a general property of nanobodies®, as they have already been used successfully as highly specific probes in antigen capturing and intracellular imaging (59,60).

Here, we have demonstrated the successful use of an Ss-LrpB-specific nanobody® (Nb9) in ChIP in *S. solfataricus*. A high-affinity interaction between the nanobody® and its cognate antigen [K_D in the nM range as routinely observed (28)] warrants a specific and efficient immunoprecipitation of the target nucleoprotein complex from the chromatin. However, it is clear that the exact epitope recognized by the antibody is also of crucial importance, and nanobodies® are no exception to this rule. Indeed the nanobodies®, like mAbs, need to be carefully screened. This is illustrated with two other Ss-LrpB specific nanobodies® (Nb1 and Nb11) with similar good affinity characteristics as the Nb9 (i.e. K_D in low nM range) but targeting a different epitope. These two Ss-LrpB-specific nanobodies® failed in ChIP, as their antigen binding provokes a clear dissociation of the SsLrpB from its DNA (Figure 3). Hence, the epitope should be preferentially located not only outside the DNA-binding domain of the protein but also outside the regions used to interact with (other) partner chromatin proteins, and these are not always known in advance. It is possible to increase the chances to retrieve 'ChIP-able' nanobodies® by selecting during phage display pannings on truncated protein constructs lacking the DNA-binding domain as done here or by selecting on cross-linked DNA–protein complexes. Finally, the use of nanobodies® has the advantage that the vast majority of them are directed to conformational epitopes, which increases the specificity and decreases the background and false-positive signal after immunoprecipitation. The chance is indeed higher that a binder to a linear epitope also interacts with a mimetic peptide.

The weakness of the nanobody®-based ChIP technology is that a specific nanobody® needs to be identified for each target. This can be avoided by using an epitope-tagging approach, where a unique peptide tag (e.g. GFP, hemagglutinin, GST, myc, FLAG) for which ChIP-able antibodies are available is knocked-in in the target gene, preferentially by homologous recombination (14). Such tagging workflow is available, for example, in model organisms *Saccharomyces cerevisae* or *E. coli* (61) and the halophilic archaeon *Halobacterium salinarum* (14). For those systems where a GFP has been introduced as a tag, a GFP binding nanobody® could be used for ChIP. This GFP-specific nanobody® has an excellent track record for intracellular targeting and for immune precipitation from cells expressing fluorescent DNA-binding proteins as well (58,62,63). Although the homologous recombination of tagged genes replacing the endogenous genes avoids the overexpression of recombinant proteins that are naturally of low abundance within the cell, the presence of an unnatural C- or N-terminal tag at the target protein might lead to complications, such as an induced loss of function by mislocalization, or multimerization and aggregation of the GFP-tagged protein. Therefore, it is probably safer and more relevant to avoid the strategy of tagged gene product. In addition, for higher eukaryotes and many (extremophilic) archaeal organisms for which genetic tools have not been developed yet or only work in the hands of specialists, homologous recombination may be less practicable. The advantage of the method proposed

here is that it is applicable to any organism. We, therefore, prefer the standard ChIP technology using dedicated antibodies, where mAbs have been substituted by nanobodies®. As aforementioned, the generation of antigen-specific nanobodies® is not a bottleneck for high-throughput ChIP experiments, as they are straightforward to generate in a short time. We use a fast immunization scheme with multiple antigens in one camel or llama. The following library construction and identification of antigen-specific nanobodies® requires only ~2 weeks each. Hence, antigen-specific nanobodies® against >100 different antigens can be isolated by one researcher per year. The subsequent microarray or deep sequencing and the interpretation of the data is much more time consuming. Thus, the work presented here paves the way for a more widespread use of nanobodies® in ChIP-chip and ChIP-seq approaches to analyse genome-wide binding of any desired chromatin-associated protein in any organism.

Interestingly, the shape of the ChIP-chip profiles for the autoregulatory binding of Ss-LrpB, for which three binding sites are present in the promoter region, has led to the identification of additional novel low-affinity operator sites in the *Ss-lrpB* ORF. Supplementary binding of transcription factors to coding regions is not uncommon and has been previously observed for another archaeal Lrp-like transcription factor from *Methanocaldococcus jannaschii* called Ptr2 (64). In this case, the additional site was located at the promoter-proximal side of the gene (position +7) at a reasonable distance from the main operator sites. In contrast, the auxiliary Ss-LrpB sites are located almost 400-bp downstream of the promoter Box1. This situation is reminiscent of the *E. coli* Lac repressor, which binds to a site 401-bp downstream of the main operator site (65). Simultaneous binding of the main operator O_1 and the auxiliary operator O_2 by a single Lac repressor tetramer induces the formation of a DNA loop and contributes to transcriptional repression. Possibly, Ss-LrpB binding to both operator regions (upstream of the ORF and at the 3′-end of the ORF) also alters the local conformation of the DNA and might even cause DNA looping. In any case, Box4 and Box5 binding is expected to contribute to autoregulation by increasing the local concentration of the transcription factor.

Thus, the discovery of the novel Ss-LrpB binding sites within the *Ss-LrpB* ORF is a nice illustration of the capacity of nanobodies® in ChIP-chip to rapidly identify novel operator sites.

SUPPLEMENTARY DATA

Supplementary Data are available at NAR Online: Supplementary Tables 1 and 2 and Supplementary Figure 1.

ACKNOWLEDGEMENTS

FUNDING

REFERENCES

1. Park,P.J. (2009) ChIP-seq: advantages and challenges of a maturing technology. *Nat. Rev. Genet.*, **10**, 669–680.
2. Ren,B., Robert,F., Wyrick,J.J., Aparicio,O., Jennings,E.G., Simon,I., Zeitlinger,J., Schreiber,J., Hannett,N., Kanin,E. *et al.* (2000) Genome-wide location and function of DNA binding proteins. *Science*, **290**, 2306–2309.
3. Buck,M.J. and Lieb,J.D. (2004) ChIP-chip: considerations for the design, analysis, and application of genome-wide chromatin immunoprecipitation experiments. *Genomics*, **83**, 349–360.
4. Grainger,D.C., Overton,T.W., Reppas,N., Wade,J.T., Tamai,E., Hobman,J.L., Constantinidou,C., Struhl,K., Church,G. and Busby,S.J. (2004) Genomic studies with Escherichia coli MelR protein: applications of chromatin immunoprecipitation and microarrays. *J. Bacteriol.*, **186**, 6938–6943.
5. Lee,T.I., Johnstone,S.E. and Young,R.A. (2006) Chromatin immunoprecipitation and microarray-based analysis of protein location. *Nat. Protoc.*, **1**, 729–748.
6. Schoppee Bortz,P.D. and Wamhoff,B.R. (2011) Chromatin immunoprecipitation (ChIP): revisiting the efficacy of sample preparation, sonication, quantification of sheared DNA, and analysis via PCR. *PLoS One*, **6**, e26015.
7. Lee,T.I., Rinaldi,N.J., Robert,F., Odom,D.T., Bar-Joseph,Z., Gerber,G.K., Hannett,N.M., Harbison,C.T., Thompson,C.M., Simon,I. *et al.* (2002) Transcriptional regulatory networks in Saccharomyces cerevisiae. *Science*, **298**, 799–804.
8. Harbison,C.T., Gordon,D.B., Lee,T.I., Rinaldi,N.J., Macisaac,K.D., Danford,T.W., Hannett,N.M., Tagne,J.B., Reynolds,D.B., Yoo,J. *et al.* (2004) Transcriptional regulatory code of a eukaryotic genome. *Nature*, **431**, 99–104.
9. Massie,C.E. and Mills,I.G. (2008) ChIPping away at gene regulation. *EMBO Rep.*, **9**, 337–343.
10. Wade,J.T., Struhl,K., Busby,S.J. and Grainger,D.C. (2007) Genomic analysis of protein-DNA interactions in bacteria: insights into transcription and chromosome organization. *Mol. Microbiol.*, **65**, 21–26.
11. Sala,C., Grainger,D.C. and Cole,S.T. (2009) Dissecting regulatory networks in host-pathogen interaction using chIP-on-chip technology. *Cell Host Microbe*, **5**, 430–437.
12. Schmid,A.K., Reiss,D.J., Pan,M., Koide,T. and Baliga,N.S. (2009) A single transcription factor regulates evolutionarily diverse but functionally linked metabolic pathways in response to nutrient availability. *Mol. Syst. Biol.*, **5**, 282.
13. Schmid,A.K., Pan,M., Sharma,K. and Baliga,N.S. (2011) Two transcription factors are necessary for iron homeostasis in a salt-dwelling archaeon. *Nucleic Acids Res.*, **39**, 2519–2533.
14. Wilbanks,E.G., Larsen,D.J., Neches,R.Y., Yao,A.I., Wu,C.Y., Kjolby,R.A. and Facciotti,M.T. (2012) A workflow for genome-wide mapping of archaeal transcription factors with ChIP-seq. *Nucleic Acids Res.*, **40**, e74.
15. Sikder,D. and Kodadek,T. (2005) Genomic studies of transcription factor-DNA interactions. *Curr. Opin. Chem. Biol.*, **9**, 38–45.
16. Ponzielli,R., Boutros,P.C., Katz,S., Stojanova,A., Hanley,A.P., Khosravi,F., Bros,C., Jurisica,I. and Penn,L.Z. (2008)

Optimization of experimental design parameters for high-throughput chromatin immunoprecipitation studies. *Nucleic Acids Res.*, **36**, e144.

17. Das,P.M., Ramachandran,K., vanWert,J. and Singal,R. (2004) Chromatin immunoprecipitation assay. *Biotechniques*, **37**, 961–969.

18. Egelhofer,T.A., Minoda,A., Klugman,S., Lee,K., Kolasinska-Zwierz,P., Alekseyenko,A.A., Cheung,M.S., Day,D.S., Gadel,S., Gorchakov,A.A. *et al.* (2011) An assessment of histone-modification antibody quality. *Nat. Struct. Mol. Biol.*, **18**, 91–93.

19. Kimura,H., Hayashi-Takanaka,Y., Goto,Y., Takizawa,N. and Nozaki,N. (2008) The organization of histone H3 modifications as revealed by a panel of specific monoclonal antibodies. *Cell Struct. Funct.*, **33**, 61–73.

20. Xie,Z., Hu,S., Qian,J., Blackshaw,S. and Zhu,H. (2011) Systematic characterization of protein-DNA interactions. *Cell. Mol. Life Sci.*, **68**, 1657–1668.

21. Yu,D., Ellis,H.M., Lee,E.C., Jenkins,N.A., Copeland,N.G. and Court,D.L. (2000) An efficient recombination system for chromosome engineering in Escherichia coli. *Proc. Natl Acad. Sci. USA*, **97**, 5978–5983.

22. Butland,G., Peregrin-Alvarez,J.M., Li,J., Yang,W., Yang,X., Canadien,V., Starostine,A., Richards,D., Beattie,B., Krogan,N. *et al.* (2005) Interaction network containing conserved and essential protein complexes in *Escherichia coli*. *Nature*, **433**, 531–537.

23. Cho,B.K., Knight,E.M. and Palsson,B.O. (2006) PCR-based tandem epitope tagging system for Escherichia coli genome engineering. *Biotechniques*, **40**, 67–72.

24. Berkner,S. and Lipps,G. (2008) Genetic tools for Sulfolobus spp.: vectors and first applications. *Arch. Microbiol.*, **190**, 217–230.

25. Leigh,J.A., Albers,S.V., Atomi,H. and Allers,T. (2011) Model organisms for genetics in the domain Archaea: methanogens, halophiles, Thermococcales and Sulfolobales. *FEMS Microbiol. Rev.*, **35**, 577–608.

26. Hamers-Casterman,C., Atarhouch,T., Muyldermans,S., Robinson,G., Hamers,C., Songa,E.B., Bendahman,N. and Hamers,R. (1993) Naturally occurring antibodies devoid of light chains. *Nature*, **363**, 446–448.

27. Muyldermans,S., Baral,T.N., Cortez-Retamozo,V., De Baetselier,P., De Genst,E., Kinne,J., Leonhardt,H., Magez,S., Nguyen,V.K., Revets,H. *et al.* (2009) Camelid immunoglobulins and nanobody technology. *Vet. Immunol. Immunopathol.*, **128**, 178–183.

28. Nguyen,V.K., Desmyter,A. and Muyldermans,S. (2001) Functional Heavy-chain antibodies in Camelidae. *Adv. Immunol.*, **79**, 261–295.

29. Muyldermans,S. (2001) Single domain camel antibodies: current status. *J. Biotechnol.*, **74**, 277–302.

30. Harmsen,M.M. and De Haard,H.J. (2007) Properties, production, and applications of camelid single-domain antibody fragments. *Appl. Microbiol. Biotechnol.*, **77**, 13–22.

31. Peeters,E., Thia-Toong,T.L., Gigot,D., Maes,D. and Charlier,D. (2004) Ss-LrpB, a novel Lrp-like regulator of Sulfolobus solfataricus P2, binds cooperatively to three conserved targets in its own control region. *Mol. Microbiol.*, **54**, 321–336.

32. Brinkman,A.B., Ettema,T.J., de Vos,W.M. and van der Oost,J. (2003) The Lrp family of transcriptional regulators. *Mol. Microbiol.*, **48**, 287–294.

33. Peeters,E. and Charlier,D. (2010) The Lrp family of transcription regulators in archaea. *Archaea*, **2010**, 750457.

34. Peeters,E., Albers,S.V., Vassart,A., Driessen,A.J. and Charlier,D. (2009) Ss-LrpB, a transcriptional regulator from *Sulfolobus solfataricus*, regulates a gene cluster with a pyruvate ferredoxin oxidoreductase-encoding operon and permease genes. *Mol. Microbiol.*, **71**, 972–988.

35. Peeters,E., Willaert,R., Maes,D. and Charlier,D. (2006) Ss-LrpB from Sulfolobus solfataricus condenses about 100 base pairs of its own operator DNA into globular nucleoprotein complexes. *J. Biol. Chem.*, **281**, 11721–11728.

36. Peeters,E., Hoa,B.T., Zegers,I., Charlier,D. and Maes,D. (2005) Overexpression, purification, crystallization and preliminary X-ray diffraction analysis of the C-terminal domain of Ss-LrpB, a

37. Brinkman,A.B., Bell,S.D., Lebbink,R.J., de Vos,W.M. and van der Oost,J. (2002) The Sulfolobus solfataricus Lrp-like protein LysM regulates lysine biosynthesis in response to lysine availability. *J. Biol. Chem.*, **277**, 29537–29549.

38. Conrath,K.E., Lauwereys,M., Galleni,M., Matagne,A., Frere,J.M., Kinne,J., Wyns,L. and Muyldermans,S. (2001) Beta-lactamase inhibitors derived from single-domain antibody fragments elicited in the camelidae. *Antimicrob. Agents Chemother.*, **45**, 2807–2812.

39. Saerens,D., Kinne,J., Bosmans,E., Wernery,U., Muyldermans,S. and Conrath,K. (2004) Single domain antibodies derived from dromedary lymph node and peripheral blood lymphocytes sensing conformational variants of prostate-specific antigen. *J. Biol. Chem.*, **279**, 51965–51972.

40. Enoru-Eta,J., Gigot,D., Thia-Toong,T.L., Glansdorff,N. and Charlier,D. (2000) Purification and characterization of Sa-lrp, a DNA-binding protein from the extreme thermoacidophilic archaeon *Sulfolobus acidocaldarius* homologous to the bacterial global transcriptional regulator Lrp. *J. Bacteriol.*, **182**, 3661–3672.

41. Brock,T.D., Brock,K.M., Belly,R.T. and Weiss,R.L. (1972) Sulfolobus: a new genus of sulfur-oxidizing bacteria living at low pH and high temperature. *Arch. Microbiol.*, **84**, 54–68.

42. She,Q., Singh,R.K., Confalonieri,F., Zivanovic,Y., Allard,G., Awayez,M.J., Chan-Weiher,C.C., Clausen,I.G., Curtis,B.A., De Moors,A. *et al.* (2001) The complete genome of the crenarchaeon Sulfolobus solfataricus P2. *Proc. Natl Acad. Sci. USA*, **98**, 7835–7840.

43. Toedling,J., Skylar,O., Krueger,T., Fischer,J.J., Sperling,S. and Huber,W. (2007) Ringo–an R/Bioconductor package for analyzing ChIP-chip readouts. *BMC Bioinformatics*, **8**, 221.

44. Zhu,L.J., Gazin,C., Lawson,N.D., Pages,H., Lin,S.M., Lapointe,D.S. and Green,M.R. (2010) ChIPpeakAnno: a Bioconductor package to annotate ChIP-seq and ChIP-chip data. *BMC Bioinformatics*, **11**, 237.

45. Livak,K.J. and Schmittgen,T.D. (2001) Analysis of relative gene expression data using real-time quantitative PCR and the 2(-Delta Delta C(T)) Method. *Methods*, **25**, 402–408.

46. De Genst,E., Silence,K., Ghahroudi,M.A., Decanniere,K., Loris,R., Kinne,J., Wyns,L. and Muyldermans,S. (2005) Strong in vivo maturation compensates for structurally restricted H3 loops in antibody repertoires. *J. Biol. Chem.*, **280**, 14114–14121.

47. Enoru-Eta,J., Gigot,D., Glansdorff,N. and Charlier,D. (2002) High resolution contact probing of the Lrp-like DNA-binding protein Ss-Lrp from the hyperthermoacidophilic crenarchaeote Sulfolobus solfataricus P2. *Mol. Microbiol.*, **45**, 1541–1555.

48. Matsunaga,F., Forterre,P., Ishino,Y. and Myllykallio,H. (2001) In vivo interactions of archaeal Cdc6/Orc1 and minichromosome maintenance proteins with the replication origin. *Proc. Natl Acad. Sci. USA*, **98**, 11152–11157.

49. Robinson,N.P., Dionne,I., Lundgren,M., Marsh,V.L., Bernander,R. and Bell,S.D. (2004) Identification of two origins of replication in the single chromosome of the archaeon Sulfolobus solfataricus. *Cell*, **116**, 25–38.

50. Orlando,V. (2000) Mapping chromosomal proteins in vivo by formaldehyde-crosslinked-chromatin immunoprecipitation. *Trends Biochem. Sci.*, **25**, 99–104.

51. Giresi,P.G., Kim,J., McDaniell,R.M., Iyer,V.R. and Lieb,J.D. (2007) FAIRE (Formaldehyde-Assisted Isolation of Regulatory Elements) isolates active regulatory elements from human chromatin. *Genome Res.*, **17**, 877–885.

52. Rhodius,V.A. and Wade,J.T. (2009) Technical considerations in using DNA microarrays to define regulons. *Methods*, **47**, 63–72.

53. Bernander,R. and Poplawski,A. (1997) Cell cycle characteristics of thermophilic archaea. *J. Bacteriol.*, **179**, 4963–4969.

54. Soppa,J. (2011) Ploidy and gene conversion in Archaea. *Biochem. Soc. Trans.*, **39**, 150–154.

55. Bailey,T.L., Boden,M., Buske,F.A., Frith,M., Grant,C.E., Clementi,L., Ren,J., Li,W.W. and Noble,W.S. (2009) MIME SUITE: tools for motif discovery and searching. *Nucleic Acids Res.*, **37**, W202–W208.

56. Peeters,E., Wartel,C., Maes,D. and Charlier,D. (2007) Analysis of the DNA-binding sequence specificity of the archaeal

transcriptional regulator Ss-LrpB from *Sulfolobus solfataricus* by systematic mutagenesis and high resolution contact probing. *Nucleic Acids Res.*, **35**, 623–633.

57. Flajnik,M., Deschacht,N. and Muyldermans,S. (2011) A case of convergence: Why did a simple alternative to canonical antibodies arise in sharks and camels? *PLoS Biol.*, **9**, e1001120.

58. Monegal,A., Ami,D., Martinelli,C., Huang,H., Aliprandi,M., Capasso,P., Francavilla,C., Ossolengo,G. and de Marco,A. (2009) Immunological applications of single domain llama recombinant antibodies isolated from a naïve library. *Protein Eng. Des. Sel.*, **22**, 273–280.

59. Rothbauer,U., Zolghadr,K., Muyldermans,S., Schepers,A., Cardoso,M.C. and Leonhardt,H. (2008) A versatile nanotrap for biochemical and functional studies with fluorescent fusion proteins. *Mol. Cell. Proteomics*, **7**, 282–289.

60. Rothbauer,U., Zolghadr,K., Tillib,S., Nowak,D., Schermaelleh,L., Gahl,A., Backmann,N., Conrath,K., Muyldermans,S., Cardoso,M.C. *et al.* (2006) Targeting and tracing of antigens in living cells. *Nat. Methods*, **3**, 887–889.

61. Sung,M.-K., Ha,C.W. and Huh,W.K. (2008) A vector system for efficient and economical switching of C-terminal epitope tags in *Saccharomyces cerevisiae*. *Yeast*, **25**, 301–311.

62. Bergbauer,M., Kalla,M., Schmeinck,A., Gobel,C., Rothbauer,U., Eck,S., Benet-Pages,A., Strom,T.M. and Hammerschmidt,W. (2010) CpG-methylation regulates a class of Epstein-Barr virus promoters. *PLoS Pathog.*, **6**, e1001114.

63. Munoz,I.M., Hain,K., Declais,A.C., Gardiner,M., Toh,G.W., Sanchez-Pulido,L., Heuckmann,J.M., Toth,R., Macartney,T., Eppink,B. *et al.* (2009) Coordination of structure-specific nucleases by human SLX4/BTBD12 is required for DNA repair. *Mol. Cell*, **35**, 116–127.

64. Ouhammouch,M., Langham,G.E., Hausner,W., Simpson,A.J., El-Sayed,N.M. and Geiduschek,E.P. (2005) Promoter architecture and response to a positive regulator of archaeal transcription. *Mol. Microbiol.*, **56**, 625–637.

65. Oehler,S., Eismann,E.R., Kramer,H. and Muller-Hill,B. (1990) The three operators of the lac operon cooperate in repression. *EMBO J.*, **9**, 973–979.